Remote sensing of lake and river ice

Chapter · January 2015

CITATIONS
69

READS
3,118

4 authors:

Claude Duguay
University of Waterloo
376 PUBLICATIONS **7,034** CITATIONS
SEE PROFILE

Monique Bernier
Institut National de la Recherche Scientifique
254 PUBLICATIONS **2,677** CITATIONS
SEE PROFILE

Yves Gauthier
Institut National de la Recherche Scientifique
76 PUBLICATIONS **891** CITATIONS
SEE PROFILE

Alexei Kouraev
Paul Sabatier University - Toulouse III
100 PUBLICATIONS **2,974** CITATIONS
SEE PROFILE

12 Remote sensing of lake and river ice

Claude R. Duguay[1], Monique Bernier[2], Yves Gauthier[2] and Alexei Kouraev[3]

[1] *University of Waterloo, Waterloo, Ontario, Canada*
[2] *Centre Eau, Terre, Environnement, Québec, Canada*
[3] *Laboratoire d'Etudes en Géophysique et Océanographie Spatiales (LEGOS), Toulouse, France*

Summary

Lake and river ice play an important role in the biological, chemical, and physical processes of cold region freshwater. The presence of freshwater ice also has many economic implications, ranging from hydroelectricity and transportation (e.g., duration of ice-road and open-water shipping seasons) to the occurrence and severity of ice-jam flooding that can cause serious damage to infrastructure and property. In addition to its significant influence on bio-physical and socio-economic systems, freshwater ice is also a sensitive indicator of climate variability and change.

Documented trends and variability in freshwater ice conditions have largely been related to air temperature changes. Long-term trends observable from ground-based records reveal increasingly later freeze-up and earlier break-up dates, closely corresponding to increasing air temperature trends, but with greater sensitivity at the more temperate latitudes. Broad spatial patterns in these trends are also related to major atmospheric circulation patterns originating from the Pacific and Atlantic oceans, such as the El Niño-La Niña/Southern Oscillation, the Pacific North American pattern, the Pacific Decadal Oscillation, and the North Atlantic Oscillation/Arctic Oscillation.

Despite the wide-ranging influences of freshwater ice and its robustness as an indicator of climate change, a dramatic reduction in ground-based observational recordings has occurred globally since the 1980s. Consequently, satellite remote sensing has assumed a greater role in observing lake ice and river ice. This chapter provides an overview of the recent progress on remote sensing of lake and river ice. For lake ice, topics reviewed comprise the determination of:

1 ice cover concentration, extent and phenology;
2 ice types;
3 ice thickness and snow on ice;
4 snow/ice surface temperature; and
5 grounded and floating ice covers on shallow Arctic and sub-Arctic lakes.

Remote Sensing of the Cryosphere, First Edition. Edited by M. Tedesco.

Companion Website: www.wiley.com/go/tedesco/cryosphere

Regarding remote sensing of river ice, topics covered include:

1 the determination of ice extent, ice phenology, ice types, ice jams, flooded areas, ice thickness, and surface flow velocities; and
2 the incorporation of SAR-derived ice information into a GIS-based system for river-flow modeling and flood forecasting.

The chapter concludes with an outlook on anticipated developments, in light of recent and upcoming satellite missions.

12.1 Introduction

Lake and river ice play an important role in the biological, chemical, and physical processes of cold region freshwater. The presence of freshwater ice also has many economic implications, ranging from hydroelectricity and transportation (e.g., duration of ice-road and open-water shipping seasons) to the occurrence and severity of ice-jam flooding, which can cause serious damage to infrastructure and property (Prowse *et al.*, 2011c). Freshwater ice is estimated to cover a total area of 1.7×10^6 km^2 over the Northern Hemisphere (determined at peak thickness, north of the January 0°C isotherm, excluding the Greenland ice sheet) and a volume of 1.6×10^3 km^3 (Brooks *et al.*, 2013; Figure 12.1). The estimated area of freshwater ice is nearly equal to that of the Greenland ice sheet, and its volume to that of snow on land.

Lakes that form a seasonal ice cover are a major component of the terrestrial landscape. They cover approximately 2% of the Earth's land surface, with the majority of them located in the Northern Hemisphere (Brown and Duguay, 2010). Estimates of their areal coverage can reach up to 40–50% in some regions of the Arctic and sub-Arctic. Lakes have the highest evaporation rates of any high latitude terrestrial surface (Rouse *et al.*, 2008a). Their frequency and size greatly influence the magnitude and timing of landscape-scale evaporative and sensible heat inputs to the atmosphere, and they are important to regional climatic and meteorological processes. Shallow lakes warm quickly in spring and have very high evaporation rates until they freeze in autumn. Large lakes take a substantially longer period to warm, but stay ice-free (or partly ice-free) into early winter, and their total evaporation amounts are significantly greater (Rouse *et al.*, 2005).

The duration of lake ice, in particular, controls the seasonal heat budget of lake systems, thus determining the magnitude and timing of evaporation (Rouse *et al.*, 2008b). The presence (or absence) of ice cover on lakes during the winter months also has an effect on both regional climate and weather events (e.g., thermal moderation and lake-effect snow) (Brown and Duguay, 2010). Monitoring of lake ice is therefore critical to our skill at forecasting high-latitude weather, climate, and river runoff. Recent investigations, indeed, emphasize the importance of considering lake ice cover for modeling the energy and water balance of high-latitude river basins, for regional climate modeling, and for improving numerical weather prediction in regions where lakes occupy a significant fraction of the landscape

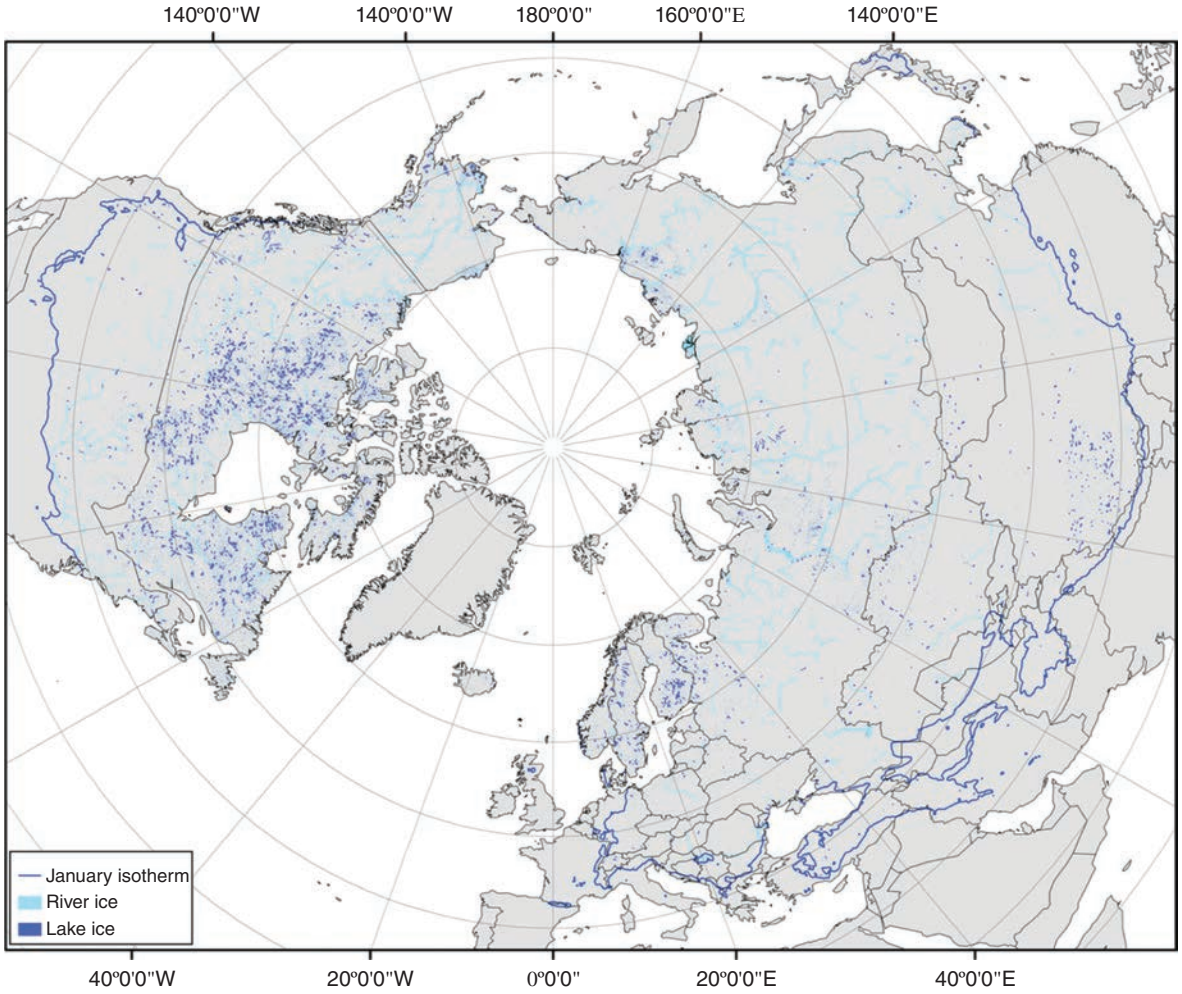

Figure 12.1 Approximate areal extent of freshwater ice in the Northern Hemisphere at peak thickness, north of the January 0°C isotherm, excluding areas of perennial land ice (from Brooks *et al.*, 2013). The water body mask used is from the Global Lake and Wetlands Database (GLWD). (Lehner and Doll, 2004. Reproduced with permission of Elsevier).

(Lindström *et al.*, 2010; Kheyrollah Pour *et al.*, 2012; Martynov *et al.*, 2012; Zhao *et al.*, 2012).

River ice also affects an extensive portion of the global hydrologic system, particularly in the Northern Hemisphere, where major ice covers develop on 29% of the total river length and seasonal ice affects 58% (Prowse *et al.*, 2007). For large rivers in cold continental regions, such as the Lena and lower Mackenzie, or at higher latitudes, such as the Yukon, ice conditions can persist for more than half the year over the entire river length (Prowse *et al.*, 2011a). In contrast, rivers with more temperate headwaters only have sections (e.g., 73% of Ob River length) that experience such long-term ice effects. For these and other rivers of the Northern Hemisphere, ice duration and break-up exert a significant control

on the timing and magnitude of extreme hydrologic events such as low flows and floods (Prowse *et al.*, 2007).

River geomorphology, vegetation regimes, and nutrient/sediment fluxes that support aquatic ecosystems are especially sensitive to changes in the severity and timing of river ice break-up (Prowse *et al.*, 2011c). Given the broad ecological and socio-economic significance of river ice, scientific concern has been expressed about how future changes in climate might affect river-ice regimes (IGOS, 2007).

In addition to its significant influence on bio-physical and socio-economic systems, freshwater ice is also a sensitive indicator of climate variability and change. Documented trends and variability in freshwater ice conditions have largely been related to air temperature changes. Long-term trends observable from ground-based records reveal increasingly later freeze-up and earlier break-up dates, closely corresponding to increasing air temperature trends, but with greater sensitivity at the more temperate latitudes (Brown and Duguay, 2010; Prowse *et al.*, 2011b). Broad spatial patterns in these trends are also related to major atmospheric circulation patterns originating from the Pacific and Atlantic oceans, such as the El Niño-La Niña/Southern Oscillation, the Pacific North American pattern, the Pacific Decadal Oscillation, and the North Atlantic Oscillation/Arctic Oscillation (see Bonsal *et al.*, 2006; Prowse *et al.*, 2011b for details).

Despite the wide-ranging influences of freshwater ice and its robustness as an indicator of climate change, a dramatic reduction in ground-based observational recordings has occurred globally since the 1980s (Lenormand *et al.*, 2002; Duguay *et al.*, 2006; IGOS, 2007; Prowse *et al.*, 2011a; Jeffries *et al.*, 2012). Satellite remote sensing provides the necessary means to increase the spatial coverage and temporal frequency of ground-based observations. This chapter provides an overview of the recent literature on remote sensing of lake and river ice, and builds on a previous review by Jeffries *et al.* (2005). For a comprehensive review of lake ice and river ice characteristics, properties and processes, the reader is invited to consult Jeffries *et al.* (2012). Remote sensing of lake ice is reviewed first followed by river ice. The chapter concludes with an outlook on anticipated developments in light of recent and upcoming satellite missions.

12.2 Remote sensing of lake ice

Remote sensing of freshwater ice is a topic that has received little attention when compared to other elements of the cryosphere. In this section, we review the main developments that have recently taken place in satellite remote sensing of lake ice, more specifically:

1 ice cover concentration, extent and phenology;
2 ice types;
3 ice thickness and snow on ice;
4 snow/ice surface temperature; and
5 grounded and floating ice covers on shallow Arctic and sub-Arctic lakes.

12.2.1 Ice concentration, extent and phenology

Ice concentration is the fraction of the water surface that is covered by ice. It is typically reported as a percentage (0 to 100% ice), a fraction (0 to 1), or in tenths (0/10 to 10/10). Ice concentration on lakes is not usually determined at the satellite pixel-scale, as is done operationally for sea ice from passive microwave-based algorithms. Rather, it is estimated over various areas of a lake, as is done for the production of ice charts by the National Oceanic and Atmospheric Administration (NOAA) for the Great Lakes of southern Canada/northern United States, or over the entire lake surface, as done by the Canadian Ice Service (CIS) (Duguay *et al.*, 2011).

Ice extent defines a section of a water body as either ice-covered or ice-free. From remote sensing data, each pixel is usually attributed a single class value for ice (i.e., not discriminating for ice types) and one for open water, as done in NOAA's Interactive Multisensor Snow and Ice Mapping System (IMS) 4 km resolution grid daily product (Helfrich *et al.*, 2007) and the National Aeronautics and Space Administration's (NASA) 500 m Moderate Resolution Imaging Spectroradiometer (MODIS) snow products (Hall *et al.*, 2002). Extent is frequently reported in terms of area (in km^2) covered by ice.

"Ice phenology" is the term used to describe the seasonal cycle of lake ice cover. It encompasses the freeze-up and break-up periods and, by extent, ice cover duration. "Freeze-up" and "break-up" are often used interchangeably with "ice on" and "ice off". Although freeze-up and break-up are often reported in the literature to occur on specific calendar dates, they rather represent processes or sequences of processes. As stated by Jeffries *et al.* (2012):

> " … *freeze-up can be viewed as the period of time between initial ice formation and establishment of a complete ice cover, and break-up as the period of time between the exposure of bare ice (once all snow has melted) and the complete clearance of the ice cover.*"

Table 12.1 provides definitions for ice phenology variables from a remote sensing perspective at the pixel level, and for entire lakes or lake sections. The terminology presented in this table could be adopted as a basis for remote sensing of ice phenology. This would remove some of the existing confusion regarding the meaning of freeze-up and break-up, particularly when comparing remote sensing-derived dates against ground-based observations and numerical lake ice model output.

12.2.1.1 Optical remote sensing

To date, operational methods to determine ice concentration and extent have largely relied on the visual (or semi-automated) interpretation of optical and, to a lesser extent, microwave imagery. Such is the case for the creation of the IMS and Canadian Ice Service (CIS) ice products (see Duguay *et al.*, 2011 for details), and NOAA ice charts (or ice analysis product) of the Great Lakes (Figure 12.2).

Table 12.1 Definition of ice phenology variables at per pixel level and for entire lake or lake section (Kang *et al.*, 2012. Reproduced under Creative Commons Attribution Licence 3.0).

	Pixel level	**Entire lake or lake section**
Freeze-up Period	**Freeze onset (FO)**: First day of the year on which the presence of ice is detected in a pixel and remains until ice-on. **Ice-on**: Day of the year on which a pixel becomes totally ice-covered. **Freeze duration (FD)**: number of days between freeze-onset and ice-on dates.	Complete freeze over (CFO): Day of the year when all pixels become totally ice-covered.
Break-up period	**Melt onset (MO)**: First day of the year on which generalized spring melt begins in a pixel. **Ice-off**: Day of the year on which a pixel becomes totally ice-free. **Melt duration (MD)**: numbers of days between melt-onset and ice-off dates.	Water clear of ice (WCI): Day of the year when all pixels become totally ice-free.
Ice season	**Ice cover duration (ICDp)**: number of days between ice-on and ice-off dates.	**Ice cover duration (ICDe)**: number of days between CFO and WCI.

The three products are generated using imagery obtained from a range of satellite sensors operating at different frequencies. As an example, the 4 km grid resolution IMS product incorporates a wide variety of satellite imagery (e.g., AVHRR, GOES, SSM/I), as well as derived mapped products (e.g., USAF Snow/Ice Analysis, AMSU) and surface observations (see Helfrich *et al.*, 2007 for details). Ice phenology (freeze-up, break-up and ice cover duration) anomalies have recently been derived from the IMS product for the largest lakes of the Arctic (Duguay *et al.*, 2011, 2012, 2013).

Few algorithms have been developed to automatically map lake ice cover from optical (visible to mid-infrared) satellite data. One algorithm, known as Snowmap, has been devised to operationally generate snow data products from the MODIS sensor onboard of NASA's Aqua and Terra satellites. The products provide information on snow-covered land and ice on inland water at spatial resolutions of 500 m and 0.05° at daily, eight-day, and monthly temporal resolutions (monthly products are only generated at 0.05°). The Snowmap algorithm may experience difficulties in detecting the presence of lake ice in areas where snow cover is patchy due to wind redistribution, a situation often encountered during the early winter period on lakes found at northernmost latitudes. However, the performance of the Snowmap algorithm over lake ice is a topic that has yet to be fully investigated.

MODIS snow data products with a spatial resolution of 500 m have been utilized recently as part of climate-related investigations. Brown and Duguay (2012) assessed the utility of the MODIS daily snow product (Collection 5) from Aqua and Terra for determining lake ice phenology at the sub-grid cell level of the

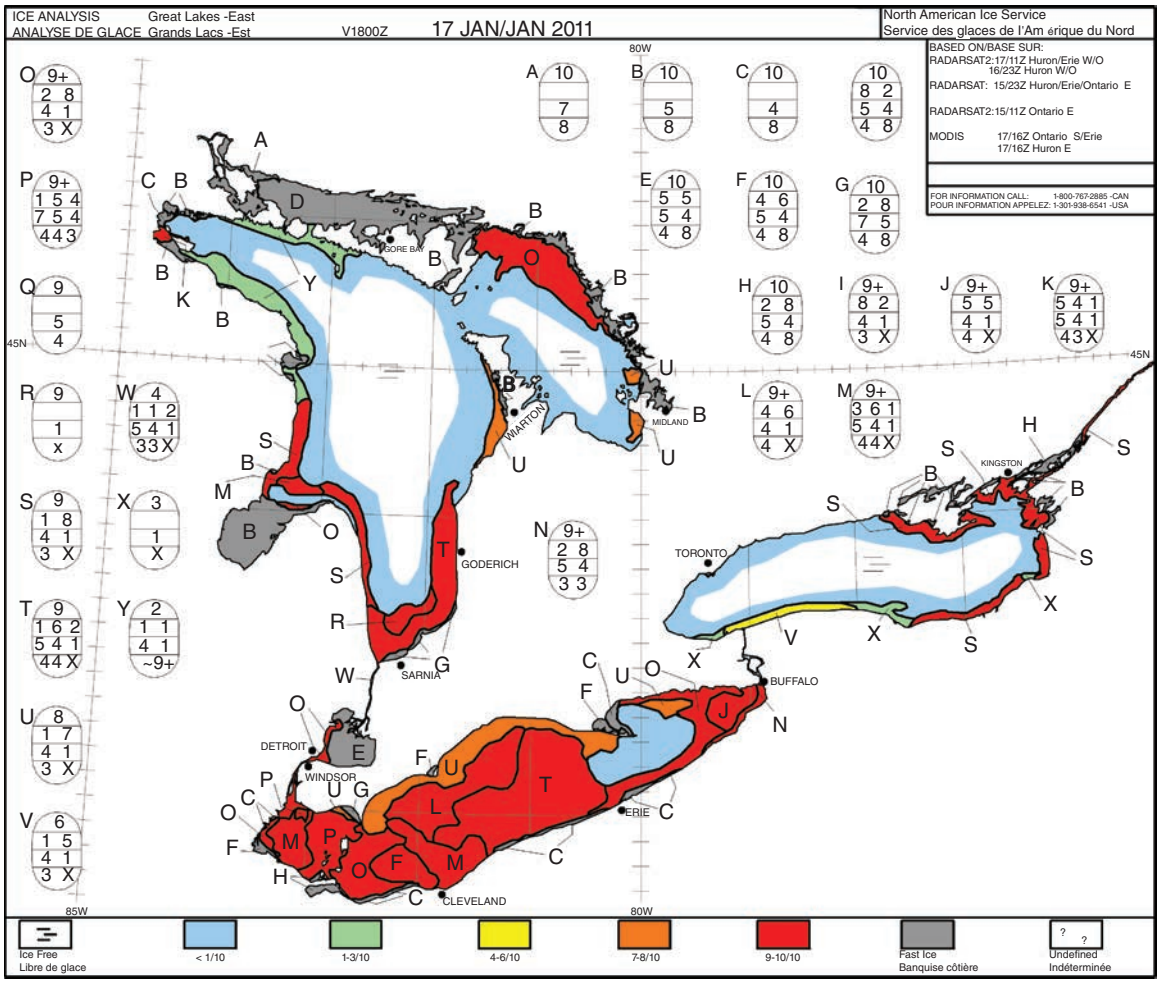

Figure 12.2 Ice analysis (chart) product of the eastern Great Lakes (Lake Ontario, Lake Erie, and Lake Huron) on 17 January 2011, constructed from the interpretation of RADARSAT-1/2 and MODIS imagery by ice analysts of the US National Ice Center (NIC). (US National Ice Center http://www.natice.noaa.gov/products/great_lakes.html).

North American Regional Reanalysis (NARR) 32-km grid product. The NARR product provided atmospheric forcing variables for lake ice model simulations with the Canadian Lake Ice Model (CLIMo; Duguay *et al.*, 2003). Both IMS 4 km and MODIS 500 m products were found to be useful for detecting ice-off dates when compared to CLIMo output. However, the MODIS product was advantageous for detecting ice-on, mainly due to the finer resolution and resulting spatial detail (Brown and Duguay, 2012).

Kropáček *et al.* (2013) used eight-day MODIS to analyze the ice phenology of 59 large lakes on the Tibetan Plateau for the period 2001–2010. The authors report that ice cover duration shows high variability due to both climatic and local factors,

and that freeze-up dates appear to be more thermally determined than break-up for the studied lakes.

An algorithm based on image thresholding of reflectance has been presented for extracting lake ice phenology events from a historical satellite record, Advanced Very High Resolution Radiometer (AVHRR; 1.1 km spatial resolution) imagery (Latifovic and Pouliot, 2007). The development of the algorithm was motivated by interest in extending existing *in situ* observational records of 36 Canadian lakes (Duguay *et al.*, 2006) and to develop records for six additional lakes in Canada's far north for the period 1985–2004. A strong agreement (i.e., similar ice trends over the overlapping period) between freeze-up and break-up dates obtained from the AVHRR record and *in situ* observations was observed, suggesting that the two data sources are a useful complement to each other. The algorithm presented by Latifovic and Pouliot (2007) is not sensor-specific and is, therefore, claimed to be applicable to data from other optical sensors such as MetOp/AVHRR, MODIS, MERIS (MEdium Resolution Imaging Spectrometer), and SPOT/VGT (Système Pour l'Observation de la Terre/VEGETATION).

While imagery from optical sensors is highly desirable for monitoring lake ice, the presence of cloud cover, which can be extensive during some periods of the year, as well as late fall/early winter darkness (or low sun angle) experienced at high latitudes, limit its usefulness during the freeze-up period, particularly when applying automated algorithms to satellite data (e.g., MODIS Snowmap). Given these limitations, investigations have also focused on the development of approaches to monitor ice cover from microwave scatterometry, radiometry, and altimetry, and from synthetic aperture radar (SAR).

12.2.1.2 Microwave remote sensing

Microwave remote sensing provides the capability to obtain ice phenology parameters under cloudy and polar darkness conditions. Algorithms that rely on the temporal evolution of backscatter (scatterometry and altimetry) and brightness temperature, or a combination of both, have recently been developed to monitor ice cover conditions on large lakes. High temporal sampling over large areas (at times twice daily or better) is possible with some of the satellite sensors operating at microwave frequencies (e.g., passive radiometers and scatterometers). This is, however, to the detriment of spatial resolution (several km to tens of km), which is much higher for SAR systems (1 m to about 100 m).

Using data from the SeaWinds scatterometer on board the NASA's QuikSCAT satellite (operational from June 1999 until November 2009), Howell *et al.* (2009) developed an algorithm to map the spatial distribution of ice phenology parameters on Great Bear Lake (GBL) and Great Slave Lake (GSL), Northwest Territories, Canada. Ku-band backscatter coefficients σ° (VV) from QuikSCAT (enhanced at 4 km spatial resolution) can be used to detect melt onset, ice-off and freeze onset (ice-on) dates. In winter, σ° exhibits relatively high returns, whereas melt onset is marked by a strong decrease in σ°.

Following the first significant downturn in the QuikSCAT σ° temporal evolution, the σ° begins a series of up and downturn oscillations. The first oscillation (i.e., up-turn and down-turn) is related to freeze-thaw processes. The sharp drop in QuikSCAT σ° after this period marks the date when the lake becomes clear of ice (ice-off). The QuikSCAT σ° then increases sharply from the relatively low open-water σ° values to higher σ° values, to indicate freeze onset (ice-on). Observed changes in σ° above or below certain threshold values form the basis of the algorithm developed by Howell *et al.* (2009). Results from the application of the algorithm to GBL and GSL have revealed contrasting patterns in ice phenology parameters within and between the two lakes (2000 – 2006 period), with ice cover duration lasting five weeks longer on GBL, and the ice regime of GSL being significantly influenced by water inflow from Slave River to the south.

More recently, Kang *et al.* (2012) developed an approach similar to that of Howell *et al.* (2009), but using daily time series of brightness temperature from the Advanced Microwave Scanning Radiometer – Earth Observing System (AMSR-E). The study shows that 18.7 GHz H-pol is the most suitable channel for detecting ice phonological events (freeze-onset/melt-onset and ice-on/ice-off dates as well as ice cover duration; see Table 12.1) on GBL and GSL. The algorithm proposed tracks changes in brightness temperature above or below predefined threshold values to detect ice dates.

A comparison of dates for several ice phenology parameters derived from other satellite remote sensing products (e.g., NOAA IMS, QuikSCAT from the study of Howell *et al.* (2009)) show that AMSR-E 18.7 GHz H-pol (or sensors operating onboard of other satellite platforms at a similar frequency) provides a promising means for routinely monitoring ice phenology on large northern lakes. The same algorithm concept could be applied to historical records of the Scanning Multi-channel Microwave Radiometer (SMMR) and Special Sensor Microwave/Imager (SSM/I), to reconstruct ice conditions on GBL and GSL since 1979.

In addition to examining the value of scatterometry and radiometry individually, potential also exists for monitoring ice cover on northern lakes, by exploiting the synergy of more than 20 years of radar altimetric and passive microwave data to improve spatial and temporal coverage. A dedicated methodology for ice discrimination has been developed and tested for the Caspian and Aral seas, as well as for the lakes Ladoga, Onega and Baikal (Kouraev *et al.*, 2003, 2007a, 2007b, 2008, and in press). The approach uses the simultaneous nadir-looking active and passive data from several altimetric missions (TOPEX/Poseidon, Jason-1, Envisat and GFO), complemented by passive microwave SSM/I data to discriminate ice from open water (Figure 12.3).

Combination of the two types of satellite observations is beneficial, due to the wide spatial coverage and good temporal resolution offered by SSM/I, and the high radiometric sensitivity and along-track spatial resolution of the altimeters. By analyzing this data, it is possible to define specific dates of ice events (the first appearance of ice, the formation of a stable ice cover, the first appearance of open water and the complete disappearance of ice) for the water bodies of interest.

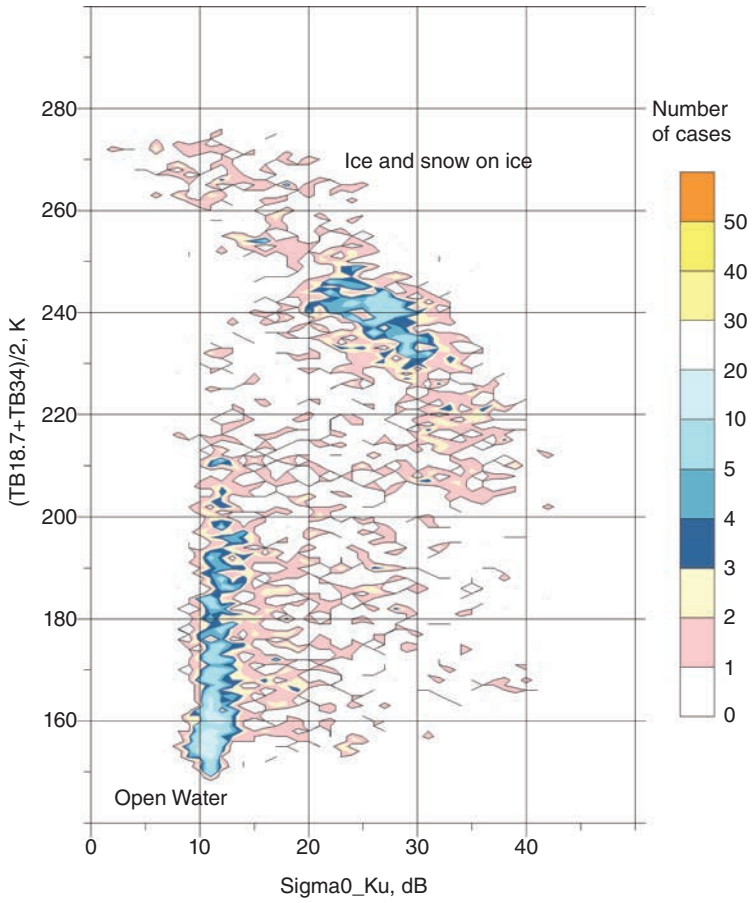

Figure 12.3 Frequency distribution (number of cases; total number of observations (n) = 3, 130) of Envisat radar altimeter backscatter observations (Sigma0_Ku in decibel, dB) versus passive (TB18.7 + TB34)/2 microwave observations (degrees Kelvin, K) for Cycles 11 to 30 (5 November 2002 to 4 October 2004) over Lake Baikal, Russia. Two well-defined clusters are easily identifiable, making it possible to discriminate open water from ice cover.

In most cases, it is possible to define ice event dates using these maps with a five-day temporal resolution, and an uncertainty of ± 2.5 days. Such an approach enhances the potential of microwave measurements for ice studies, and can be used reliably to extend the existing time series available for coastal stations, as well as to create new time series for regions that were not previously covered by continuous *in situ* observations.

Co-polarized (HH and VV) SAR data from the ERS-1/2 (C-band), JERS-1 (L-band), RADARSAT-1/2 (C-band) and Envisat ASAR (C-band) sensors have also been analyzed, mostly through visual interpretation, to map changes in lake ice cover in response to climate over the last decade or so at Arctic locations. For example, Mueller *et al.* (2009) used SAR data acquired in late summer to show that five lakes located at the northern tip of Ellesmere Island (Nunavut, Canada) experienced significant reductions in summer ice cover from 1992 to 2007, with some lakes transitioning from perennially to annually ice-covered conditions following the warm El Niño year of 1998.

In a separate study, Cook and Bradley (2010) analyzed RADARSAT (HH-pol) and LANDSAT Thematic Mapper (TM)/Enhanced Thematic Mapper Plus (ETM+) imagery (115 SAR and 19 LANDSAT images) to evaluate recent (1997–2007) changes in the ice cover of Upper and Lower Murray Lakes (81°20′N, 69°30′W), also situated on Ellesmere Island, during the melt period. Similar to the results reported in Mueller *et al.* (2009), the authors suggest that the observed ice melt at Upper and Lower Murray Lakes, due to recent warming in the high Arctic, has forced the lakes near a threshold from a state characterized by perennial ice cover to the current state, which includes seasonal melting of lake ice.

The potential of multi-polarized (co-, cross-, and quad-polarization) SAR data has recently been examined to automatically map lake ice cover during the break-up (melt) period (Geldsetzer *et al.*, 2010; Sobiech and Dierking, 2013). Geldsetzer *et al.* (2010) analyzed RADARSAT-2 SAR imagery for monitoring ice cover during spring melt on lakes located in the Old Crow Flats, Yukon, Canada. The authors were successful at identifying initial break-up with a simple threshold applied to HH backscatter data (>81% accuracy) and the main break-up period with a threshold on cross-polarized (HV) data (66–97%).

Sobiech and Dierking (2013) evaluated the performance of the unsupervised k-means classification in a binary classification of ice cover and open water on lakes and river channels of the central Lena Delta, northern Siberia. K-means is an unsupervised image classification approach frequently used for mapping river ice types (see section 12.3.2). Using six TerraSAR-X (X-band, single HH co-pol) and three RADARSAT-2 images (C-band, quad-pol HH, VV, HV, and VH simultaneously) obtained during spring, 2011, Sobiech and Dierking found that the performance of the k-means classification is comparable to that of a fixed-threshold approach. Application of a low-pass filter prior to the classification of river channels, and a closing filter on the classification results of lakes, strongly improved the overall k-means classification results.

12.2.2 Ice types

Unlike ice cover concentration and extent, classification of lake ice types has been the object of very few investigations. This is in striking contrast to river ice, for which classification of ice types has been the topic of several publications (see section 12.3.2). This situation likely stems from the fact that knowledge of river ice types is important not only for public safety and navigation, as is also the case for lake ice, but most notably for the prediction and mitigation of river ice jams (Bérubé *et al.*, 2009).

SAR data is useful for obtaining some information about the internal structure of ice (texture) due to the ability of the microwave signal to penetrate ice (Hall *et al.*, 1994) under dry snow conditions. The most comprehensive data set of coincident ice type and radar observations over lake ice was collected during the 1997 Great LAkes Winter Experiment (GLAWEX'97; Nghiem and Leshkevich, 2007).

As part of this experiment, a C-band polarimetric scatterometer operated by the Jet Propulsion Laboratory (JPL) was installed on separate occasions on two icebreaker vessels for periods of two weeks each (February and March, 1997) in order to gather backscatter signatures of various ice types (new ice, pancake ice, consolidated ice, stratified ice, brash ice, and lake ice with crusted snow) and open water on Lake Superior at incidence angles from 0–60°. The scatterometer measurements included incidence angles and polarizations of spaceborne SAR instruments on ERS, RADARSAT, and Envisat satellites.

The ultimate goal of GLAWEX'97 was to compile a library of radar signatures, together with *in situ* observations, of ice types that could be used with the interpretation of spaceborne SAR data, acquired concurrently with Earth Resource Satellite 2 (ERS-2; VV) and RADARSAT-1 ScanSAR (HH) imagery, for ice classification and mapping (Nghiem and Leshkevich, 2007). Using the library of backscatter signatures, Leshkevich and Nghiem (2007) were able successfully to identify and map different ice types through a supervised classification technique. However, wind speed and direction was found to confound the discrimination between open water and ice, since RADARSAT-1 and ERS-2 provide single frequency, single polarization data. Cross-polarization data (e.g., RADARSAT-2 and TerraSAR-X) are less sensitive to wind effects than co-polarized data and, therefore, could be seen as optimal for discriminating between open water and ice cover on windy days. However, Geldsetzer *et al.* (2010) recently reported that the signal from open water surfaces (as well as that from lake ice) can be at or below the noise floor, making cross-polarized data of limited use. Sobiech and Dierking (2013) conclude that HH-polarized images are best suited for separation of ice and water surfaces.

12.2.3 Ice thickness and snow on ice

Lake ice has been shown to respond to changing climate conditions, particularly changes in air temperature and snow accumulation (Brown and Duguay, 2011). Trends and variability in ice phenology are typically associated with variations in air temperatures, while trends in ice thickness tend to be associated more with changes in snow cover (Brown and Duguay, 2010). During the ice growth season, the dominant factors that control the thickening of lake ice are temperature and snowfall. Once ice has formed, snow accumulation on the ice surface slows the growth of ice below due to the insulating properties as a result of the lower thermal conductivity (thermal conductivity of snow, 0.08–0.54 $Wm^{-1}K^{-1}$ vs 2.24 $Wm^{-1}K^{-1}$ for ice; Sturm *et al.*, 1997).

Snow mass can also change the composition of the ice by promoting snow ice development, and hence influence the thickness of the ice cover (Brown and Duguay, 2010). Observations of ice thickness and snow on ice (depth, mass) are required for both climate monitoring, and for evaluating and improving models of lake-ice growth. Microwave sensors provide the capabilities for estimating ice thickness and snow on ice over broad areas and with high temporal coverage. However, few studies have explored this potential.

Until very recently, no approach had been developed to estimate ice thickness on large lakes from satellite remote sensing. The potential of passive microwave data for ice thickness determination had, however, been previously demonstrated in an airborne study by Hall *et al.* (1981), using a limited number of field observations. Other studies have shown that ERS or RADARSAT C-band SAR could be used to determine ice thickness in northern shallow lakes that freeze to bed (see section 12.2.5), when combined with optical data that can provide estimates of lake depth (e.g., Duguay and Lafleur, 2003).

Lately, Kang *et al.* (2010) have shown that the temporal evolution of brightness temperature measurements from the AMSR-E 10.7 GHz and 18.7 GHz frequency channels during the ice growth season on Great Bear Lake (GBL) and Great Slave Lake (GSL), Canada, is strongly correlated with ice thickness as estimated with a numerical lake ice model (Duguay *et al.*, 2003). Using AMSR-E data from 2002–2007, the authors showed that over 90% of the variations in brightness temperature on GBL and GSL could be explained by the seasonal evolution of ice thickness on these lakes in winter. The strong relationship between brightness temperature at 18.7 GHz V-pol and ice growth from the lake ice model has since been explored for the development of regression-based ice thickness (ICT) retrieval algorithms (Kang *et al.*, 2014). Simple linear regression equations ($ICT_{GBL} = 3.53 \times T_B - 737.929$ for GBL $ICT_{GSL} = 2.83 \times T_B - 586.305$ for GSL) allow for the estimation of ice thickness (in cm) on a monthly basis from January to April (Figure 12.4). The transferability of the regression equations remains to be examined for other large lakes of the Northern Hemisphere (e.g., Lake Baikal, Lake Ladoga, and Lake Onega in Russia).

While some progress has been made in estimating ice thickness from coarse-resolution passive microwave data, no method has yet been developed to our knowledge for estimating snow depth or snow water equivalent (SWE) on lake ice. Duguay *et al.* (2005) have shown that traditional passive microwave algorithms used to estimate SWE over land (difference between 37 GHz and 19 GHz frequency channels) do not work when applied over lake ice. Derksen *et al.* (2009) further illustrate that 19 and 37 GHz frequencies have penetration depths ($\approx$2 at 19 GHz and 0.75 m at 37 GHz) that are strongly influenced by water beneath the ice for part of the season, but are also influenced by the ice and overlying snowpack by the end of the season.

The estimation of snow depth (and SWE) on lake ice is a challenging problem that needs to be further investigated using both passive and active microwave data acquired at Ka-/Ku-band frequencies. Kouraev *et al.* (2007a) report that snow accumulation, ice ageing (growth), and decay induce a decrease in Ku-band radar altimetry backscatter values and changes in passive microwave brightness temperature measurements (see Figure 12.3).

12.2.4 Snow/ice surface temperature

It is now well recognized that satellite observations of lake ice extent/concentration and lake surface temperature are valuable for improving numerical weather

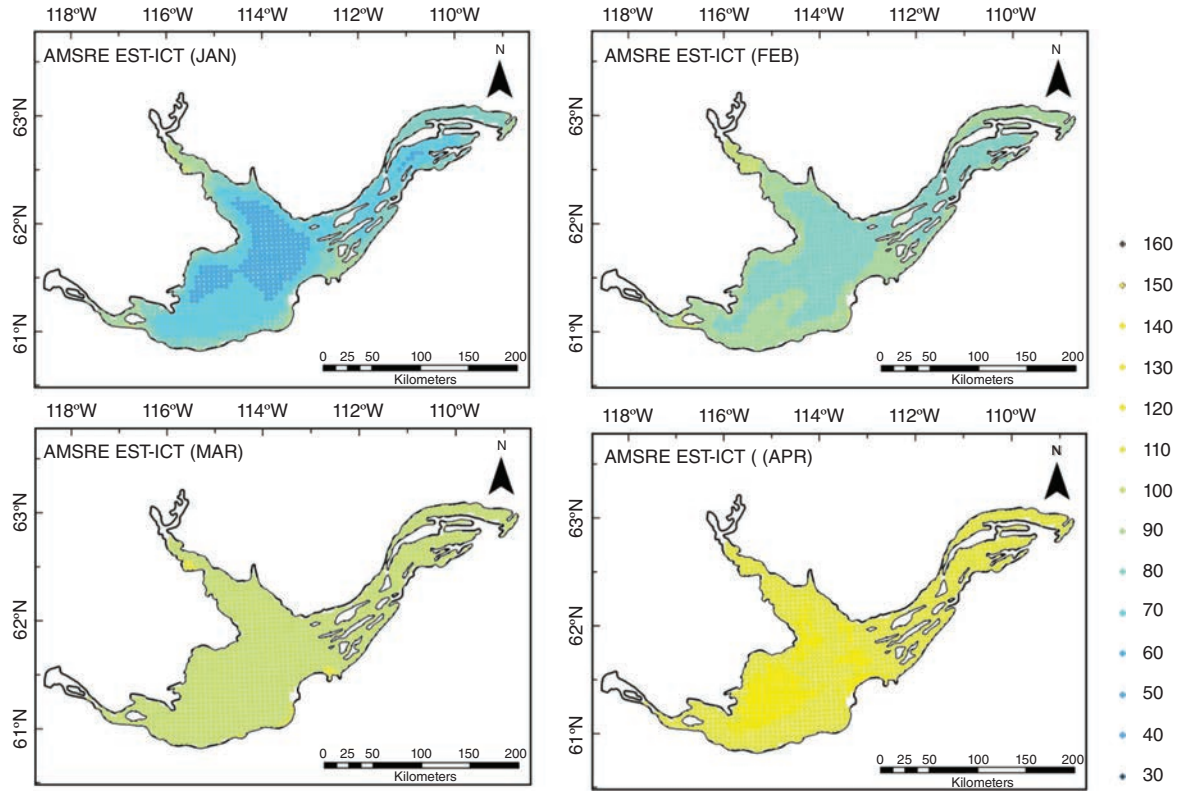

Figure 12.4 Ice thickness maps of Great Slave Lake for the months of January, February, March and April (2002 – 2009 average) derived from AMSR-E 18.7 GHz V-pol brightness temperature data (Kang *et al.*, in press. Reproduced with permission of Elsevier).

predictions in regions where lakes occupy a significant fraction of the landscape (e.g., Kheyrollah Pour *et al.*, 2012; Zhao *et al.*, 2012). Furthermore, it has been shown that lake surface temperature (LST) products derived from satellite sensors such as MODIS are useful for evaluating lake snow/ice surface temperature output simulated with one-dimensional lake models. For example, Kheyrollah Pour *et al.* (2012) showed that MODIS daily LST is helpful at identifying current limitations of the Freshwater Lake model (FLake), one of the most common lake models used as a lake parameterization scheme in numerical weather prediction (NWP) and regional climate models (RMCs), particularly regarding its lack of proper representation of snow on ice.

Compared to FLake, the Canadian Lake Ice Model (CLIMO; Duguay *et al.*, 2003), which simulates the seasonal evolution of snow cover on the lake ice surface, generates snow/ice surface temperatures that are closer to those observed with MODIS (Figure 12.5). Statistics of model performance given by the index of agreement (Ia), the root mean square error (RMSE), and mean bias error (MBE), reveal that CLIMO outperforms FLake, even if both models slightly overestimate the LSTs

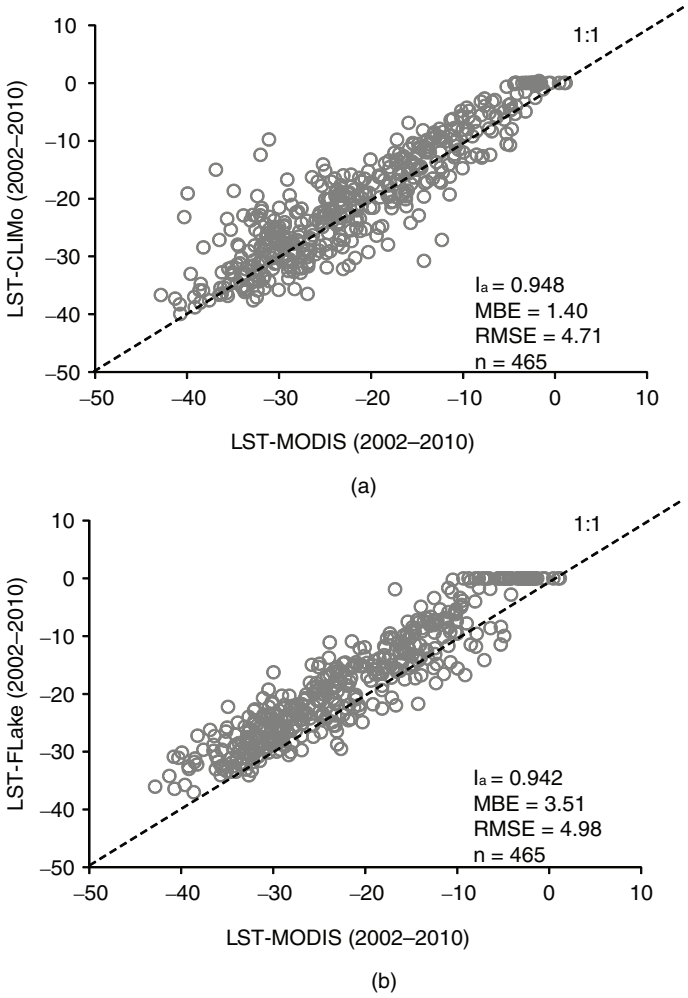

Figure 12.5 Comparison of modeled LST from (a) CLIMo and (b) FLake models with MODIS-derived LST (°C) data for ice cover seasons 2002–2010 in Back Bay (Great Slave Lake), Canada. Modified from Kheyrollah Pour *et al.*, 2012.

from MODIS. However, land/lake surface temperatures from MODIS products have been reported to suffer from a 1–2°C cold bias (ignoring the possible effect of cloud contamination) in other studies (e.g., Soliman *et al.*, 2012).

12.2.5 Floating and grounded ice: the special case of shallow Arctic/sub-Arctic lakes

Shallow lakes (less than ≈4 m deep) are a ubiquitous feature of the Arctic coastal plains of Siberia, northern Alaska and Canada. In Canada, for example, they are particularly prevalent in the Hudson Bay Lowlands and the Mackenzie River Delta region. Within the Arctic, shallow water bodies (lakes and ponds) are estimated to occupy between 15% and 50% of total land area (Duguay and Pietroniro, 2005).

There has been interest for many years in monitoring/mapping the seasonal evolution of floating and grounded ice (i.e., ice that is frozen to the bottom of the lake) of shallow lakes from remote sensing. Knowing when (i.e., the timing) and where the ice becomes grounded or remains afloat on shallow lakes during the ice growth season is relevant for climate monitoring (e.g., Arp *et al.*, 2012; Surdu *et al.*, 2014; Figure 12.6), the determination of water availability (e.g., Jeffries *et al.*, 1996; White *et al.*, 2008; Grunblatt and Atwood, 2013), and mapping of fish overwintering habitat (e.g., Hirose *et al.*, 2008; Brown *et al.*, 2010).

With Arctic climate warming, shallow tundra lakes are expected to develop thinner ice covers, likely resulting in a smaller fraction of lakes that freeze to their bed in winter (Surdu *et al.*, 2014). A shift from a grounded-ice to a floating-ice regime can initiate talik development and could potentially release large stocks of carbon previously frozen in permafrost in the form of methane (Arp *et al.*, 2012).

In SAR imagery, floating ice that contains bubbles (a typical situation for shallow tundra lakes) shows strikingly different backscatter intensities than that of ground ice. The change from high (floating ice) to low (grounded ice) backscatter during the ice growth season has been documented and explained in several investigations using C-band SAR data from ERS-1/2, RADARSAT-1, Envisat Advanced SAR alternating polarization and wide swath modes (Jeffries *et al.*, 1994; Morris *et al.*, 1995; Duguay *et al.*, 2002; Duguay and Lafleur, 2003; Brown *et al.*, 2010; Arp *et al.*, 2011, 2012; Engram *et al.*, 2012; Surdu *et al.*, 2014) and,

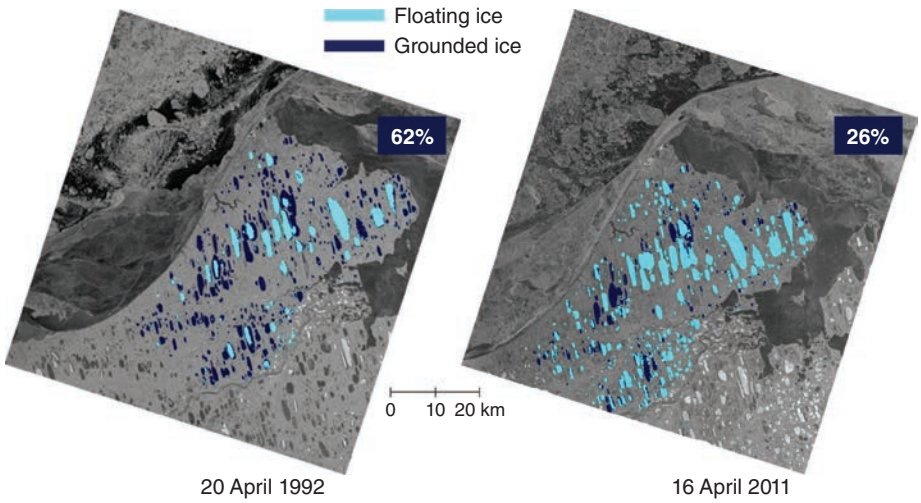

Figure 12.6 Image segmentation results (grounded ice and floating ice) of ERS-1/2 SAR acquisitions (20 April 1992 and 16 April 2011), obtained with the Iterative Region Growing with Semantics (IRGS) algorithm, as implemented in the MAp-Guided Ice Classification System (MAGIC) software (Clausi *et al.*, 2010). Ice season 1991–1992 was colder than 2010–2011, resulting in a larger number of lakes freezing to their bed (grounded) in April 1992 (62% grounded ice), compared with the same period in April 2011 (26% grounded ice).

recently, with L-band data (23.6 cm) acquired by the Japan Aerospace eXploration Agency's (JAXA) Phased-Array type L-band SAR (PALSAR) instrument aboard the Earth on the Advanced Land Observing Satellite (ALOS) (Engram *et al.*, 2012).

12.3 Remote sensing of river ice

In many northern rivers, the development of ice covers leads to important critical issues: ice jamming and, therefore, flooding of large areas; reduction of hydroelectric power at generating stations; impediment to navigation; and damage to human structures. The dynamic ice and flooding that accompany dynamic freeze-up and break-up, in particular, pose a significant risk to human life. In this section, we review advances in remote sensing of river ice, specifically:

1 the determination of ice extent, ice phenology, ice types, ice jams, flooded areas, ice thickness, and surface flow velocities and
2 the incorporation of SAR-derived ice information into a GIS-based system for river-flow modeling and flood forecasting.

12.3.1 Ice extent and phenology

Ice extent defines a section of a river as either ice-covered or ice-free, without consideration for ice types. Ice phenological parameters are determined by monitoring the evolution of ice extent along rivers from freeze onset, until water becomes clear of ice. Both optical and radar altimeter data have been used for this purpose on larger rivers. Pavelsky and Smith (2004) used daily time series of MODIS (250 m) and AVHRR (1.1 km) satellite images to monitor the spatial and temporal patterns of ice break-up along 1600 – 3300 km segments of the Lena, Ob', Yenisey, and Mackenzie rivers. The authors were able to visually identify the first day of predominantly ice-free water for ten years (1992 – 1993, 1995 – 1998, and 2000 – 2003), with a mean accuracy of 1.75 days when compared to ground-based observations. Large ice jams were also observable (see section 12.3.4 for more on this topic), particularly at confluences. However, smaller ice jams could not be detected, due to the limited spatial resolution of the imagery used. As shown in Figure 12.7, MODIS imagery can detect ice jams and flooding from the largest rivers.

In a more recent study, Chaouch *et al.* (2012) developed an automated approach that incorporates a threshold-based decision-tree image classification algorithm to determine ice extent from MODIS (visible and near-infrared bands at 250 m) on the Terra satellite. The algorithm, which generates three ice extent products (i.e., daily ice maps, weekly composite ice maps, and running cloud-free composite ice maps), was evaluated over nine ice seasons (2002 – 2010). Evaluation of the MODIS derived products for the Susquehanna River, one of the longest ($\approx$ 715 km) and widest ($\approx$ 1609 m at Harrisburg, PA) rivers in the northeastern USA, reveals

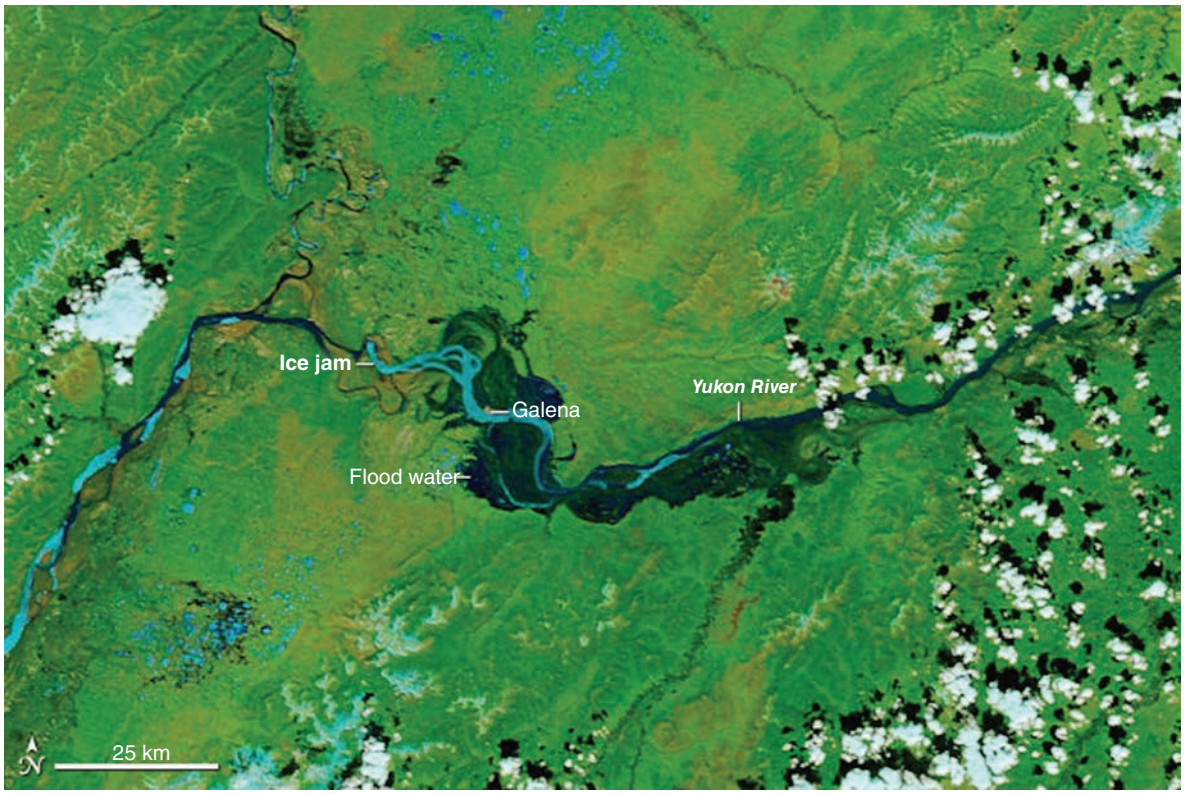

Figure 12.7 Ice jam on the Yukon River and flooding of the small town of Galena, Alaska, from the Moderate Resolution Imaging Spectroradiometer (MODIS) on NASA's Terra satellite, captured on May 28, 2013. In this color composite image, river water appears navy blue; ice appears teal; and vegetation is bright green. Clouds are white to pale blue-green, and cast shadows black. (NASA).

a good agreement with aerial photographs, *in situ* observations-based ice charts, and LANDSAT imagery (91% probability of ice detection).

Satellite radar altimetry is another tool that has recently been explored for monitoring the ice regime of large rivers. Troitskaya *et al.* (in press) propose a methodology for ice discrimination from altimetric satellite missions based on the analysis of two parameters:

a) backscatter values (ICE-2 retracker) from Ku-band (18 Hz waveform) Envisat radar altimeter data; and
b) brightness temperature differences ($dT_B = T_{B36.5} - T_{B23.8}$) from passive microwave radiometer data.

The approach has been developed and tested for the Ob' River in Russia (Troitskaya *et al.*, in press). For each crossover of the altimetric track over the main river channel, data is processed and grouped into 11 zones around selected

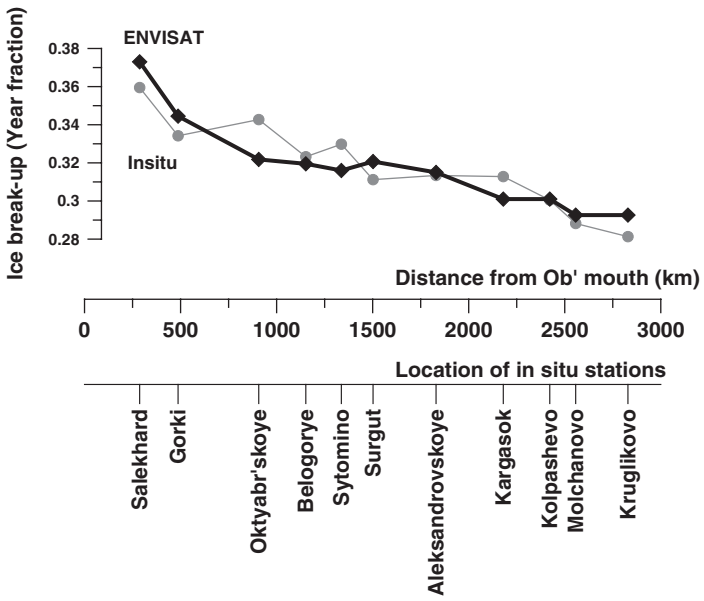

Figure 12.8 Average *in situ* (grey line, 2001 – 2011) and altimeter-derived (black line, 2002 – 2011) values of ice break-up along the main Ob' river channel between Salekhard and Novosibirsk, Russia.

ground-based stations, in order to increase the temporal resolution. The spatial variability of altimeter-derived dates of ice formation and break-up is in good agreement with ground-based observations for each zone (Figure 12.8). The algorithm and chosen threshold perform best for ice break-up detection, showing the dates of full clearance of ice, with an average bias equal to 0 and maximum bias ranging from −5 to 8 days.

12.3.2 Ice types, ice jams and flooded areas

Information on river ice types is needed for accurate hydrological forecasts to predict break-up of ice jams, and to issue timely flood warnings (Chaouch *et al.*, 2012). SAR is the preferred tool for the classification of river ice types, due to its penetrating capabilities and sensitivity to surface roughness and ice texture, particularly the size and density of volume scatterers (e.g., air bubbles) (Gherboudj *et al.*, 2007, 2010). C-band SAR at high spatial resolution (ca. 5 – 30 m) has been used successfully to map various ice types on small to medium-size rivers, or small stretches of large rivers.

Weber *et al.* (2003) used fine beam-mode RADARSAT-1 (HH) data acquired in winter and spring, 2000 and 2001, to map major ice cover types on the Peace River (northern British Columbia and Alberta, Canada). Video footage of the ice conditions on the Peace River was obtained from aerial ice observations conducted simultaneously with SAR image acquisitions. Image analysis was accomplished through visual interpretation, and by performing an unsupervised Fuzzy k-means classification applied to the RADARSAT-1 data. The unsupervised classification

produced seven classes that represented the major ice cover types observed on the Peace River. The spatial distribution of ice cover types, as generated by the ice classification, coincided generally well with airborne observations and the visual interpretation of the original RADARSAT-1 images. Weber *et al.* (2003) indicated that the location of the boundaries between the ice types appeared to be accurate, but not necessarily precise.

The work of Weber *et al.* (2003) has lead to several follow-up investigations to automatically map, via image segmentation techniques, ice cover types on large rivers. The peer-reviewed literature on the subject reveals that the development of improved methods or the adoption and validation of existing ones has mainly, if not all, taken place in Canada. For example, Töyrä *et al.* (2005) further validated the approach developed by Weber *et al.* (2003) for the lower Peace River, Alberta. Using RADARSAT-1 standard beam mode images acquired during a break-up ice jam event on April 29 and May 1, 2003, Töyrä *et al.* (2005) evaluated its use for rapid-response mapping, using minimal ground verification. After a visual comparison with aircraft observations, it was noted that ice jams, deteriorated ice and solid ice, as well as the open water leads and reaches, were mapped very well.

The RADARSAT-1 images were also used to generate ice-jam flood maps using the unsupervised Fuzzy k-means classifier. It was found that spring ice-jam flood extents could easily be delineated. Results of the study of Töyrä *et al.* (2005) showed that RADARSAT-1 images were useful for the rapid mapping of river ice break-up conditions and spring flood extent. Unterschultz *et al.* (2009) also investigated the viability of using RADARSAT-1 satellite images to characterize river ice during the winter ice growth and break-up periods (Athabasca River, Alberta, Canada). They concluded that SAR shows excellent potential for identifying ice jams, intact ice, and open water during break-up.

Further advances in the determination of river ice types from SAR show that a two-step process involving image texture and unsupervised classification with the Fuzzy k-means algorithm is the method that provides the best results to date (Gauthier *et al.*, 2007, 2008). The procedure, known as the Ice Mapping Automated Procedure from Radar data (IceMap-R; Gauthier *et al.*, 2010), allows for the fully automated segmentation of up to nine ice classes and open water areas from RADARSAT HH data. The classified ice types are then merged into the main ice types (i.e., thermal ice, juxtaposed (or agglomerated) frazil ice and consolidated ice, along with open water; Figure 12.9) and can also be converted into roughness classes (e.g., water and floating pans, smooth ice and rough ice) needed as input in hydraulic flood routing models such as River1D (She and Hicks, 2006).

The global accuracy of IceMap-R in correctly classifying the main ice types with RADARSAT HH data is consistently around 70–80% (Gauthier *et al.*, 2012). Known limitations of the automated procedure applied to co-polarization HH data include the discrimination between smooth thermal ice and water, the presence of frazil pans, the presence of melting snow or water over ice, and the presence of rapids. Jasek *et al.* (2013) showed that the accuracy obtainable with IceMap-R can be significantly increased by exploring the use of both co- and cross-polarized (HH and HV) data available from RADARSAT-2. Using a set

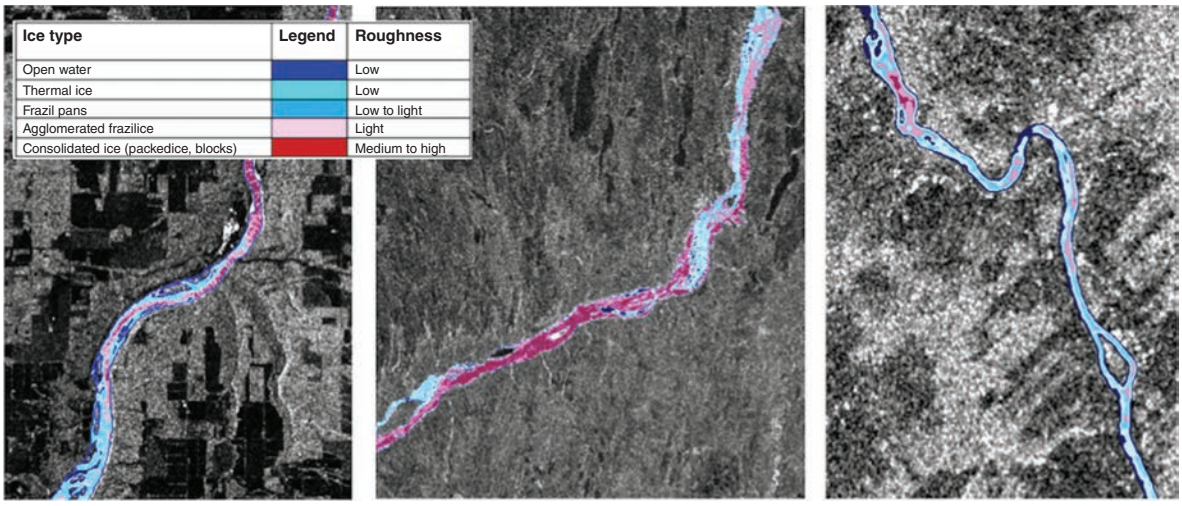

Figure 12.9 River ice types and related roughness classes derived from RADARSAT-1 HH imagery using IceMap for the Peace, Koksoak, and Chaudière rivers, Canada.

of five RADARSAT-2 images acquired for a section of the Peace River (British Columbia, Canada), the authors showed that HV is most efficient in correctly classifying water and juxtaposed ice, while HH is better for discriminating thermal ice and consolidated ice. The global accuracy achieved with this combination of polarizations is in the order of 90%. This is a significant improvement over the use of RADARSAT HH data alone (70–80%).

12.3.3 Ice thickness

Knowledge of ice thickness is important for river-ice hydraulic models. Together with ice roughness, it is one of the key ice parameters for flood routing models (She and Hicks, 2006). As part of an investigation on the evaluation of RADARSAT-1 data to characterize river ice during winter and breakup on the Athabasca River at Fort McMurray, Canada, Unterschultz *et al.* (2009) also assessed the possibility of estimating river ice thickness with C-band SAR. To determine whether a correlation did exist between ice thickness and C-band HH radar backscatter, observations of ice thickness, snow depth, and ice structure/type (e.g., thermal, juxtaposed, hummocky) were made during a field measurement campaign (February 17–19, 2004) along nine transects on the river, and compared to backscatter values extracted from fine beam mode RADARSAT-1 images acquired around the same time period (February 7 and March 2). The authors reported that a relationship did exist between ice thickness (transect average values) and mean backscatter, but that the sample size was too small for this to be considered a

conclusive demonstration of any ability to determine average ice thickness based on radar backscatter alone. Results from the study suggested that knowledge of ice structure and inclusions (i.e., bubbles) needs to be considered for developing a model for ice thickness determination using SAR images. Unterschultz *et al.* (2009) concluded that further investigations are needed before ice thickness can be determined from SAR backscatter data.

In a more recent study, Mermoz *et al.* (2013) developed a method for the retrieval of river ice thickness from RADARSAT-2 polarimetric C-band SAR data. The authors first performed a Wishart classification to derive river ice types (Mermoz *et al.*, 2009b), followed by the masking of bubble-free thermal ice and consolidated ice. These two ice types were determined to represent surface areas ranging from 29.9% to 60.4% of a given river and excluded from further analysis because their radar backscatter signature was found to be almost insensitive to thickness variations. The relationship between radar backscatter and river ice thickness measurements was then examined over the unmasked areas of the three rivers (at 70 locations in total).

For the other ice types, polarimetric entropy (a measure that captures variability in terms of scattering mechanisms) was used to obtain ice thickness estimates from RADARSAT-2 data (the fitted model explained up to 85% of the observed variance in ice thickness). A leave-one-out cross-validation was then applied to assess the accuracy of the river ice thickness estimates. The RMSE was found to be 9.2 cm, and the effective RMSE 16.6 %. However, Mermoz *et al.* (2013) suggest that the robustness of this empirical model remains to be assessed. Interferometric SAR data also provides a promising means for the retrieval of pure thermal ice thickness (Wegmuller *et al.*, 2010).

Thermal infrared imagery is another technology that shows potential for estimating thin river ice. In a recent study, airborne images from a FLIR A40M thermal camera were acquired and successfully used to estimate thickness of thin ice (<20 cm) on the St. Lawrence River, between Montreal and Quebec City, Canada. A simplified one-dimensional heat diffusion equation was solved using a finite element method to obtain ice thickness from airborne ice temperature measurements. The thermal images were also shown to provide significant details about ice floe characteristics, ice concentration, shape, size, structure, and number of floes per hectare, in addition to surface temperature and ice thickness. The approach developed in this study could be explored further to estimate thin ice of large rivers and lakes from thermal infrared data acquired by MODIS on the Terra and Aqua satellites, for example.

12.3.4 Surface flow velocities

Quantification of river surface velocity is important for understanding a wide range of biological, chemical and physical processes in northern rivers, and for the evaluation of river hydraulic models. Kääb and Prowse (2011) recently

developed a novel approach that uses river-ice debris as an index of surface water velocity. The river-ice debris are tracked over the typical time lapse of two or more image acquisitions by spaceborne optical sensors that form a data set for stereo mapping. Using a satellite stereo image pair from the Advanced Spaceborne Thermal Emission and Reflection Radiometer (ASTER) onboard the NASA Terra satellite (15 m spatial resolution and 55.3 s time lapse), a triplet stereo scene from the Panchromatic Remote Sensing Instrument for Stereo Mapping (PRISM) aboard the Japanese ALOS satellite (2.5 m spatial resolution and 45 s or 90 s lapse rate, respectively), and an IKONOS satellite stereo pair (1 m spatial resolution and 53 s time lapse), ice debris are tracked between two images. The resulting displacements are then converted to velocity, using the time interval between the stereo images.

With this approach, Kääb and Prowse were able to measure and visualize, for the first time, the almost complete surface velocity field along approximately 80 km and 40 km long reaches of the St. Lawrence and Mackenzie rivers (Canada), respectively. Surface flow velocities derived from the ALOS PRISM satellite stereo triplet for a section of the Mackenzie River are shown in Figure 12.10. The approach proposed by the authors is, indeed, very promising, but it needs to be tested for more stereo-image data sets and validated with coincident *in situ* measurements of surface flow velocity and observations of river-ice debris with shore-based or airborne cameras.

12.3.5 Incorporating SAR-derived ice information into a GIS-based system in support of river-flow modeling and flood forecasting

While satellite imagery can help monitor the evolution of ice jams, fronts, and flooded areas, there is a need to improve models to help forecast flooding and become early warning systems (e.g., Puestow *et al.*, 2004). The FRAZIL system, developed by Gauthier *et al.* (2007, 2008), is a GIS-based system designed to support winter river-flow modeling and ice-related flood forecasting. It has been tested and improved since its inception in 2005 on rivers in the province of Quebec and, more recently, on the Athabasca River, northern Alberta, Canada.

The FRAZIL system includes two major components. The first of these consists of a set of GIS tools developed in the Python programming language, for use with ArcGIS (ESRI), and the second one incorporates a series of image processing routines (IceMap-R), developed in the image-processing software Geomatica (PCI Geomatics). FRAZIL is used to help define the morphological characteristics of a river channel before hydraulic modeling, as well as to characterize the ice cover state (ice coverage, roughness and ice-jam length) and evolution (ice front progression, freeze-up completion, signs of breakup) from SAR-derived ice maps. Some of the data generated by the FRAZIL system can then be used as input into hydraulic routing models or breakup forecasting models.

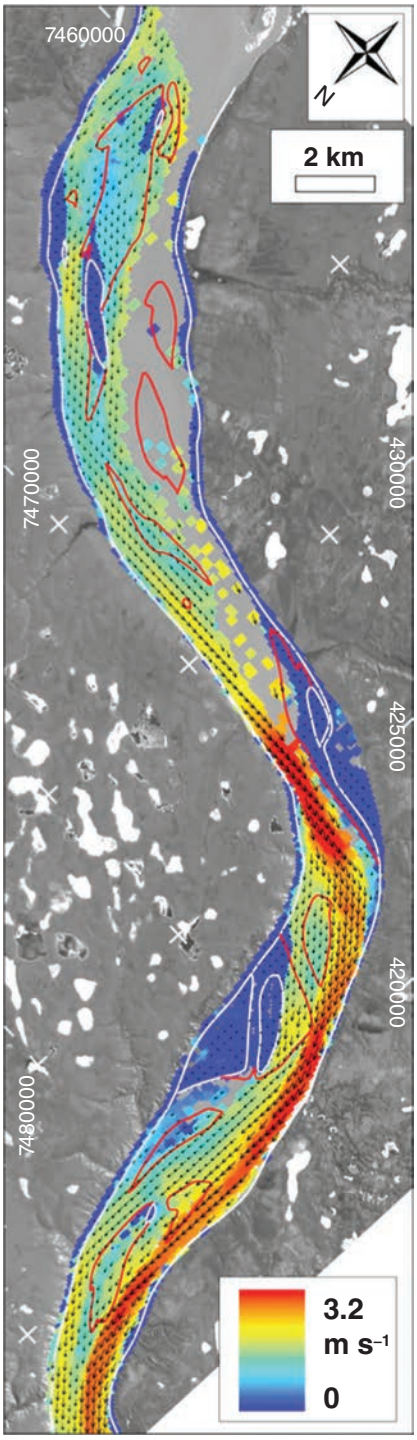

Figure 12.10 Surface flow velocities and vectors on the Mackenzie River, Canada, derived from an ALOS PRISM satellite stereo triplet of 21 May 2008 acquired at around 20:30 UTC. The red outlines indicate sand bars visible at low water level, the white lines vegetated islands and river margins assumed to be not or only slightly flooded during high water. Grey data voids in the river indicate open water without ice debris tracked. Image center latitude and longitude are approximately 67.33°N/130.70°W. Coordinate grid UTM zone 9. (Kääb, A. and Prowse, T. 2011. Reproduced with permission of John Wiley & Sons Inc).

12.4 Conclusions and outlook

Freshwater ice is one of, if not the least, studied components of the cryosphere from remote sensing. With the increasing recognition of the importance of freshwater ice as a sensitive indicator of climate variations, and its impact on ecological and human systems in a changing climate, there is a rising demand for timely information on lake and river ice conditions (e.g., timing of phenological events, ice thickness, ice jams and flooding). However, as alluded to earlier in this chapter and in recent studies, this happens at a time when ground-based observational networks have "hit bottom" in many countries of the Northern Hemisphere, to the point where they can no longer form the primary basis of observations.

In fact, the lamentable state of ground-based freshwater ice observation networks is not a recent phenomenon in countries such as Canada; this is something that began 20 – 30 years ago (e.g., Lenormand *et al.*, 2002). Unfortunately, this occurred at a time when satellite remote sensing technology was not fully ready to complement or replace ground-based observations.

As shown throughout this chapter, significant progress has taken place in remote sensing of lake and river ice over the last decade, but many of the approaches (algorithms) developed to date have not reached maturity to the extent required by the environmental modeling community (e.g., numerical weather forecasting, climate and hydrological modeling) or by public policy- and decision-makers (e.g., transportation on ice roads, prediction and mitigation of ice jams and flood warning). However, there are some signs that we are progressing in the right direction, as demonstrated in pilot studies (e.g., the assimilation of lake surface temperature and ice cover in NWP models, and the integration of SAR-derived river ice products in a GIS-based system for flood forecasting). Upcoming satellite missions, such as ESA's Sentinels (the first Sentinel was planned for launch in 2013) and Canada's RADARSAT constellation (planned for 2018), will further encourage the development and greater operational usage of remote-sensing freshwater ice products. Exciting times do lie ahead for satellite remote sensing of lake and river ice.

Acknowledgments

The work of M. Bernier and C. Duguay was supported by European Space Agency (ESA-ESRIN) Contract No. 4000101296/10/I-LG (Support to Science Element, North Hydrology Project) and Discovery Grants from the Natural Sciences and Engineering Research Council of Canada (NSERC). The early development of FRAZIL was also supported by the GEOIDE Network of Excellence, the Canadian Space Agency (CSA), and Hydro-Québec. The development of IceMAP-R was supported by the Quebec Public Safety Department, BC Hydro, and the CSA SOAR program. The research of A. Kouraev was completed within the framework

of the Russian-French cooperation GDRI "CAR-WET-SIB", PICS "BaLaLaICA", Project 13-05-91051-RFBR-a "Lakes Baikal and Ladoga – joint complex studies", French ANR "CLASSIQUE", CNES TOSCA "Lakes" and "SWOT" Projects, Russian FZP 1.5 "Kadry", and EU FP7 "MONARCH-A" projects. Finally, we wish to thank Kyung-Kuk (Kevin) Kang, Homa Kheyrollah Pour and Cristina Surdu for the production of Figures 12.4, 12.5 and 12.6, respectively.

References

Arp, C.D., Jones, B. ., Urban, F, and Grosse, G. (2011). Hydrogeomorphic processes of thermokarst lakes with grounded-ice and floating-ice regimes on the Arctic coastal plain. *Alaska, Hydrological Processes* **25**, 2422–2438.

Arp, C.D., Jones, B.M., Lu, Z., and Whitman, M.S. (2012). Shifting balance of thermokarst lake ice regimes across the Arctic Coastal Plain of northern Alaska. *Geophysical Research Letters* **39**, L16503, doi: 10.1029/2012GL052518.

Bérubé, F., Bergeron, N., Gauthier, Y., and Choquette, Y. (2009). *Investigation of the use of GPR for characterizing river ice types*. Proceedings of the 15th Workshop on the Hydraulics of Ice Covered Rivers, St. John's, Canada, June 15–17, 2009, 55–64.

Bonsal, B.R., Prowse, T.D., Duguay, C.R., and Lacroix, M.P. (2006). Impacts of large-scale teleconnections on freshwater-ice duration over Canada. *Journal of Hydrology* **330**, 340–353.

Brooks, R., Prowse, T.D., and O'Connell, I.J. (2013). Quantifying Northern Hemisphere freshwater ice. *Geophysical Research Letters* **40**, 1128–1131, doi: 10.1002/grl.50238.

Brown, L.C. and Duguay, C.R. (2010). The response and role of ice cover in lake-climate interactions. *Progress in Physical Geography* **34**, 671–704, doi: 10.1177/0309133310375653.

Brown, L.C. and Duguay, C.R. (2011). A comparison of simulated and measured lake ice thickness using a Shallow Water Ice Profiler. *Hydrological Processes* **25**, 2932–2941, doi: 10.1002/hyp.8087.

Brown, L.C. and Duguay, C.R. (2012). Modelling lake ice phenology with an examination of satellite detected sub-grid cell variability. *Advances in Meteorology* **2012**, Article ID 529064, 19 pages, doi: 10.1155/2012/529064.

Brown, R.S., Duguay, C.R., Mueller, R.P., Moulton, *et al.* (2010). Use of synthetic aperture radar to identify and characterize overwintering areas of fish in ice-covered arctic rivers: a demonstration with broad whitefish and their habitats in the Sagavanirktok River, Alaska. *Transactions of the American Fisheries Society* **139**, 1711–1722, doi: 10.1577/T09–176.1.

Chaouch, N., Temimi, M., Romanov, P., Cabrera, R., *et al.* (2012). An automated algorithm for river ice monitoring over the Susquehanna River using the MODIS data. *Hydrological Processes*, doi: 10.1002/hyp.9548.

Clausi, D., Qin, A., Chowdhury, M., Yu, P., and Maillard, P. (2010). MAGIC: Map-guided ice classification system. *Canadian Journal of Remote Sensing* **36**, S13 – S25.

Cook, T.L. and Bradley, R.S. (2010). An analysis of past and future changes in the ice cover of two High-Arctic lakes based on synthetic aperture radar (SAR) and LANDSAT imagery. *Arctic, Antarctic, and Alpine Research* **42**, 9 – 18, doi: 10.1657/1938-4246-42.1.9.

Derksen, C., Silis, A., Sturm, M., *et al.* (2009). Northwest Territories and Nunavut snow characteristics from a subarctic traverse: Implications for passive microwave remote sensing. *Journal of Hydrometeorology* **10**, 448 – 463, doi: 10.1175/2008JHM1074.1.

Duguay, C., Brown, L., Kang, K.-K., and Kheyrollah Pour, H. (2011). Lake ice. In: Richter-Menge, J., Jeffries, M.O. & Overland, J.E. (eds). *Arctic Report Card 2011*. http://www.arctic.noaa.gov/reportcard.

Duguay, C., Brown, L., Kang, K.-K., and Kheyrollah Pour, H. (2012). [Arctic]. Lake ice. [In State of the Climate in 2011]. *Bulletin of the American Meteorological Society* **93**, S156 – S158.

Duguay, C., Brown, L., Kang, K.-K., and Kheyrollah Pour, H. (2013). [Arctic]. Lake ice. [In State of the Climate in 2012]. *Bulletin of the American Meteorological Society* **94**, S152 – S154.

Duguay, C.R. and Lafleur, P.M. (2003). Estimating depth and ice thickness of shallow subarctic lakes using spaceborne optical and SAR data. *International Journal of Remote Sensing* **24**, 475 – 489.

Duguay, C.R. and Pietroniro, A. (2005). *Remote Sensing in Northern Hydrology: Measuring Environmental Change*. Geophysical Monograph 163, American Geophysical Union, Washington, DC, 160 pp., doi: 10.1029/GM163.

Duguay, C.R., Pultz, T.J., Lafleur, P.M., and Drai, D. (2002). RADARSAT backscatter characteristics of ice growing on shallow sub-arctic lakes, Churchill, Manitoba, Canada. *Hydrological Processes* **16**, 1631 – 1644.

Duguay, C.R., Flato, G.M., Jeffries, M.O., Ménard, P., *et al.* (2003). Ice cover variability on shallow lakes at high latitudes: Model simulations and observations. *Hydrological Processes* **17**, 3465 – 3483.

Duguay, C.R., Green, J., Derksen, C., English, *et al.* (2005). *Preliminary assessment of the impact of lakes on passive microwave snow retrieval algorithms in the Arctic*. Proceedings of 62nd Eastern Snow Conference, Waterloo, Ontario, Canada, June 7 – 10, 2005, 223 – 228.

Duguay, C.R., Prowse, T.D., Bonsal, B.R., Brown, R.D., *et al.* (2006). Recent trends in Canadian lake ice cover. *Hydrological Processes* **20**, 781 – 801.

Engram, M., Walter Anthony, K., Meyer, F., and Grosse, G. (2012). Synthetic aperture radar (SAR) backscatter response from methane ebullition bubbles trapped by thermokarst lake ice. *Canadian Journal of Remote Sensing* **38**, 667 – 682.

Gauthier, Y., Paquet, L.-M., Gonzalez, A., Hicks, F., *et al.* (2007). *Using the FRAZIL system in support of winter river flow modeling*. Proceedings of the 14th Workshop on the Hydraulics of Ice Covered Rivers, Quebec City, Canada, June 19 – 22, 2007, 17pp.

Gauthier, Y., Paquet, L.-M., Gonzalez, A., and Bernier, M. (2008). Using radar and GIS to support ice related flood forecasting *Geomatica* **62**, 273–285.

Gauthier, Y., Tremblay, M., Bernier, M. and Furgal, C. (2010). Adaptation of a radar-based river ice mapping technology to the Nunavik context. *Canadian Journal of Remote Sensing* **36**(S1), 168–185, doi: 10.5589/m10-018.

Gauthier, Y., Poulin, J. Bernier, M. (2012). *Rapport d'évaluation de l'algorithme ICEMAP-R (v3.0) pour la cartographie radar de la glace de rivière*. Rapport de recherche remis à la Direction de la sécurité civile, Ministère de la Sécurité publique du Québec.

Geldsetzer, T., van der Sanden, J., and Brisco, B. (2010). Monitoring lake ice during spring melt using RADARSAT-2 SAR. *Canadian Journal of Remote Sensing* **36**(S2), S391–S400.

Gherboudj, I., Bernier, M., Hicks, F., and Leconte, R. (2007). Physical characterization of air inclusions in river ice. *Cold Regions Science and Technology* **49**, 179–194.

Gherboudj, I., Bernier, M., and Leconte, R. (2010). A backscatter modelling for river ice cover: Analysis and numerical results. *IEEE Transactions on Geoscience and Remote Sensing* **48**, 1788–1798.

Grunblatt, J. and Atwood, D. (2013). Mapping lakes for winter liquid water availability using SAR on the North Slope of Alaska. *International Journal of Applied Earth Observation and Geoinformation*, 10.1016/j.jag.2013.05.006.

Hall, D.K., Foster, J.L., Chang, A.T.C., and Rango, A. (1981). Freshwater ice thickness observations using passive microwave sensors. *IEEE Transactions on Geoscience and Remote Sensing* **GE-19**, 189–193.

Hall, D.K., Fagre, D.B., Klasner, F., Linebaugh, G., *et al.* (1994). Analysis of ERS–1 synthetic aperture radar data of frozen lakes in northern Montana and implications for climate studies. *Journal of Geophysical Research* **99**, 22,473–22,482.

Hall, D.K., Riggs, G.A., Salomonson, V.V., DiGiromamo, N., *et al.* (2002). MODIS snow-cover products. *Remote Sensing of Environment* **83**, 181–194.

Helfrich, S.R., McNamara, D., Ramsay, B.H., Baldwin, T., *et al.* (2007). Enhancements to, and forthcoming developments in the Interactive Multisensor Snow and Ice Mapping System (IMS). *Hydrological Processes* **21**, 1576–1586.

Hirose, T., Kapfer, M., Bennett, J., Cott, P., *et al.* (2008). Bottomfast ice mapping and the measurement of ice thickness on tundra lakes using C-band synthetic aperture radar remote sensing. *Journal of the American Water Resources Association* **44**, 285–292.

Howell, S.E.L., Brown, L.C., Kang, K.-K., and Duguay, C.R. (2009). Variability in ice phenology on Great Bear Lake and Great Slave Lake, Northwest Territories, Canada, from SeaWinds/QuikSCAT: 2000–2006. *Remote Sensing of Environment* **113**, 816–834.

IGOS (2007). *Integrated Global Observing Strategy Cryosphere Theme Report – For the Monitoring of our Environment from Space and from Earth*. Geneva: World Meteorological Organization. WMO/TD-No. 1405. 100 p.

Jasek, M., Gauthier, Y., Poulin, J., and Bernier, M. (2013). *Monitoring of freeze-up on the Peace River at the Vermilion rapids using RADARSAT-2 SAR data*. Proceedings of the 17th Workshop on River Ice, Edmonton, Alberta, July 21–24, 2013, 29 pp.

Jeffries, M.O., Morris, K., Weeks, W.F., and Wakabayashi, H. (1994). Structural and stratigraphic features and ERS 1 synthetic aperture radar backscatter characteristics of ice growing on shallow lakes in NW Alaska, winter 1991–1992. *Journal of Geophysical Research* **99**, 22459–22471.

Jeffries, M.O., Morris, K., and Liston, G.E. (1996). A method to determine lake depth and water availability on the north slope of Alaska with spaceborne radar and numerical ice growth modeling. *Arctic* **49**, 367–374.

Jeffries, M.O., Morris, K., and Kozlenko, N. (2005). Ice characteristics and processes, and remote sensing of frozen river and lakes, In: Duguay, C.R. and Pietroniero, A. (eds). *Remote Sensing in Northern Hydrology*. AGU Monograph **163**, 63–90.

Jeffries, M.O., Morris, K., and Duguay, C.R. (2012). Floating ice: lake ice and river ice. In: Williams, R.S., Jr. and Ferrigno, J.G. (eds). *Satellite Image Atlas of Glaciers of the World – State of the Earth's Cryosphere at the Beginning of the 21st Century: Glaciers, Global Snow Cover, Floating Ice, and Permafrost and Periglacial Environments*. US Geological Survey Professional Paper 1386-A, A381–A424.

Kääb, A. and Prowse, T. (2011). Cold regions river flow observed from space. *Geophysical Research Letters* **38**, L08403, doi: 10.1029/2011GL047022.

Kang, K.-K., Duguay, C.R., Howell, S.E., Derksen, C.P., *et al*. (2010). Sensitivity of AMSR-E brightness temperatures to the seasonal evolution of lake ice thickness. *IEEE Geoscience and Remote Sensing Letters* **7**, 751–755, doi: 10.1109/LGRS.2010.2044742.

Kang, K.-K., Duguay, C.R., and Howell, S.E. (2012). Estimating ice phenology on large northern lakes from AMSR-E: Algorithm development and application to Great Bear Lake and Great Slave Lake, Canada. *The Cryosphere* **6**, 235–254, doi: 10.5194/tc-6-235-2012.

Kang, K.-K., Duguay, C.R., Lemmetyinen, J., and Gel, Y. (2014). Estimation of ice thickness on large northern lakes from AMSR-E brightness temperature measurements. *Remote Sensing of Environment* **150**, 1–19, doi: 10.1016/j.rse.2014.04.016.

Kheyrollah Pour, H., Duguay, C.R., Martynov, A., and Brown, L.C. (2012). Simulation of surface temperature and ice cover of large northern lakes with 1-D models: A comparison with MODIS satellite data and *in situ* measurements. *Tellus Series A: Dynamic Meteorology and Oceanography* **64**, 17614, doi: 10.3402/tellusa.v64i0.17614.

Kouraev A.V., Papa, F., Buharizin P.I., Cazenave, A., *et al*. (2003). Ice cover variability in the Caspian and Aral seas from active and passive satellite microwave data. *Polar Research* **22**, 43–50.

Kouraev, A.V., Semovski, S.V., Shimaraev, M.N., Mognard, N.M., *et al.* (2007a). Observations of lake Baikal ice from satellite altimetry and radiometry. *Remote Sensing of Environment* **108**, 240 – 253.

Kouraev, A.V., Semovski, S.V., Shimaraev, M.N., Mognard, N.M., *et al.* (2007b). Ice regime of lake Baikal from historical and satellite data: Influence of thermal and dynamic factors. *Limnology and Oceanography* **52**, 1268 – 1286.

Kouraev A.V., Shimaraev, M.N., Buharizin, P.I., Naumenko, M.A., *et al.* (2008). Ice and snow cover of continental water bodies from simultaneous radar altimetry and radiometry observations. *Survey in Geophysics*, doi 10.1007/s10712-008-9042-2.

Kouraev A.V., Cretaux, J.F., Zakharova, E., Mercier, F., *et al.* (in press). Seasonally-frozen lakes in boreal regions. In: Benveniste, J., Vignudelli, S., and Kostianoy, A. (eds). *Inland water altimetry*. Springer.

Kropáček, J., Maussion, F., Chen, F., Hoerz, S., *et al.* (2013). Analysis of ice phenology of lakes on the Tibetan Plateau from MODIS data. *The Cryosphere* **7**, 287 – 301.

Latifovic, R. and Pouliot, D. (2007). Analysis of climate change impacts on lake ice phenology in Canada using the historical satellite data record. *Remote Sensing of Environment* **16**, 492 – 507.

Lehner, B. and Doll, P. (2004). Development and validation of global database of lakes, reservoirs and wetlands. *Journal of Hydrology* **296**, 1 – 22, doi: 10.1016/j.jhydrol.2004.03.028.

Lenormand, F., Duguay, C.R., and Gauthier, R. (2002). Development of a historical ice database for the study of climate change in Canada. *Hydrological Processes* **16**, 3707 – 3722.

Leshkevish, G.A. and Nghiem, S.V. (2007). Satellite SAR remote sensing of Great Lakes ice cover. Part 2. Ice classification and mapping. *Journal of Great Lakes Research* **33**, 736 – 750.

Lindström, G., Pers, C.P., Rosberg, R., Strömqvist, J., *et al.* (2010). Development and test of the HYPE (Hydrological Predictions for the Environment) model – a water quality model for different spatial scales. *Hydrology Research* **41**, 295 – 319.

Martynov, A., Sushama, L., Laprise, R., Winger, K., *et al.* (2012). Interactive lakes in the Canadian Regional Climate Model, version 5: the role of lakes in the regional climate of North America. *Tellus Series A: Dynamic Meteorology and Oceanography* **64**, 16226, doi: 10.3402/tellusa.v64i0.16226.

Mermoz, S., Allain, S., Bernier, M., Pottier, E., *et al.* (2009a). Classification of river ice using polarimetric data. *Canadian Journal of Remote Sensing* **35**, 460 – 473.

Mermoz, S., Dribault, Y., Bernier, M., Allain, S., *et al.* (2009b). *Investigation of RADARSAT-2 and Terrasar-X data for river ice characterization from remote sensing*. Proceedings of the 15th Workshop on the Hydraulics of Ice Covered Rivers, St. John's, Canada, June 15 – 17, 2009, 389 – 400.

Mermoz, S., Allain-Bailhache, S., Bernier, M., Pottier, E., *et al.* (2013). Retrieval of river ice thickness from C-band PolSAR data. *IEEE Transactions on Geoscience and Remote Sensing* **99**, 1 – 11, doi: 10.1109/TGRS.2013.2269014.

Morris, K., Jeffries, M.O., and Weeks, W.F. (1995). Ice processes and growth history on Arctic and sub-Arctic lakes using ERS-1 SAR data. *Polar Record* **31**, 115–128.

Mueller, D.R., Van Hove, P., Antoniades, D., Jeffries, M.O., *et al.* (2009). High Arctic lakes as sentinel ecosystems: Cascading regime shifts in climate, ice cover, and mixing. *Limnology and Oceanography* **54**, 2371–2385.

Nghiem, S.V. and Leshkevich, G.A. (2007). Satellite SAR remote sensing of Great Lakes ice cover, Part 1. Ice backscatter signatures at C Band. *Journal of Great Lakes Research* **33**, 722–735.

Pavelsky, T. and Smith, L.C. (2004). Spatial and temporal patterns in Arctic river ice breakup observed with MODIS and AVHRR time series. *Remote Sensing of Environment* **93**, 328–338.

Prowse, T.D., Bonsal, B.R., Duguay, C.R., and Lacroix, M.P. (2007). River-ice break-up/freeze-up: A review of climatic drivers, historical trends, and future predictions. *Annals of Glaciology* **46**, 443–451.

Prowse, T., Alfredsen, K., Beltaos, S., Bonsal, B., *et al.* (2011a). Arctic freshwater ice and its climatic role. *Ambio* **40**(S1), 46–52, doi 10.1007/s13280-011-0214-9.

Prowse, T., Alfredsen, K., Beltaos, S., Bonsal, B., *et al.* (2011b). Past and future changes in lake and river ice. *Ambio* **40**(S1), 53–62, doi 10.1007/s13280-011-0216-7.

Prowse, T., Alfredsen, K., Beltaos, S., Bonsal, B., *et al.* (2011c). Effects of changes in Arctic lake and river ice. *Ambio* **40**(S1), 63–74, doi 10.1007/s13280-011-0217-6.

Puestow, T.M., Randell, C.J., Rollings, K.W., Khan, A.A., *et al.* (2004). *Near real-time monitoring of river ice in support of flood forecasting in eastern Canada: Towards the Integration of Earth observation technology in flood hazard mitigation*. Proceedings of the IEEE International Geoscience and Remote Sensing Symposium, Vol. 4, Anchorage, USA, 20–24 September 2004, 2268–2271, doi: 10.1109/IGARSS.2004.1369736.

Rouse, W.R., Binyamin, J., Blanken, P.D., Bussières, N., *et al.* (2005). Role of northern lakes in a regional energy balance. *Journal of Hydrometeorology* **6**, 291–305.

Rouse, W.R., Blanken, P.D., Duguay, C.R., Oswald, C.J., *et al.* (2008a). The Influence of lakes on the regional heat and water balance of the central Mackenzie River Basin. Chapter 18 in *Cold Region Atmospheric and Hydrologic Studies: The Mackenzie GEWEX Experience, Volume 1: Atmospheric Dynamics*, Springer-Verlag, 309–325.

Rouse, W.R., Blanken, P.D., Duguay, C.R., Oswald, C.J., *et al.* (2008b). Climate-lake interactions. Chapter 8 in *Cold Region Atmospheric and Hydrologic Studies: The Mackenzie GEWEX Experience, Volume 2: Hydrologic Processes*, Springer-Verlag, 139–160.

She, Y. and Hicks, F.E. (2006). Modeling ice jam release waves with consideration for ice effects. *Journal of Cold Regions Science and Technology* **45**, 137–147.

Sobiech, J. and Dierking, W. (2013). Observing lake- and river-ice decay with SAR: advantages and limitations of the unsupervised k-means classification approach. *Annals of Glaciology* **54**, 65–72, doi: 10.3189/2013AoG62A037.

Soliman, A., Duguay, C., Saunders, W., and Hachem, S. (2012). Pan-Arctic land surface temperature from MODIS and AATSR: Product development and intercomparison. *Remote Sensing* **4**, 3833–3856; doi: 10.3390/rs4123833.

Sturm, M., Holmgren, J., König, M., and Morris, K. (1997). The thermal conductivity of seasonal snow. *Journal of Glaciology* **43**, 26–41.

Surdu, C., Duguay, C.R., Brown, L.C., and Fernández Prieto, D. (2014). Response of ice cover on shallow lakes of the North Slope of Alaska to contemporary climate conditions (1950–2011): radar remote sensing and numerical modeling data analysis. *The Cryosphere* **8**, 167–180, doi: 10.5194/tc-8-167-2014.

Töyrä, J., Pietroniro, A., Carter, T., and Beltaos, S. (2005). *RADARSAT-1 SAR classification of breakup river ice condition and ice jam flooding*. Proceedings of the 26th Canadian Symposium on Remote Sensing, Wolfville, Canada, June 14–16, 2005, 97–98.

Troitskaja Y., Lebedev, S.A., Kostianoy, A.G., Kouraev, A.V., *et al.* (in press). Rivers and reservoirs in boreal zone of Eurasia. In: Benveniste, J., Vignudelli, S., and Kostianoy, A. (eds). *Inland water altimetry*. Springer.

Unterschultz, K.D., van der Sanden, J., and Hicks, F.E. (2009). Potential of RADARSAT-1 for the monitoring of river ice: Results of a case study on the Athabasca River at Fort McMurray, Canada. *Cold Regions Science and Technology* **55**, 238–248.

Weber, F., Nixon, D., and Hurley, J. (2003). Semi-automated classification of river ice types on the Peace River using RADARSAT-1 synthetic aperture radar (SAR) imagery. *Canadian Journal of Civil Engineering* **30**, 11–27.

Wegmuller, U., Santoro, M., Werner, C., Strozzi, T., *et al.* (2010). *Estimation of ice thickness of tundra lakes using ERS-ENVISAT cross-interferometry*. Proceedings of the IEEE International Geoscience and Remote Sensing Symposium, Honolulu, USA, 25–30 July 2010, 316–319, doi: 10.1109/IGARSS.2010.5649026.

White, D.M., Prokein, P., Chambers, M.K., Lilly, M.R., *et al.* (2008). Use of synthetic aperture radar for selecting Alaskan lakes for winter water use. *Journal of the American Water Resources Association* **44**, 276–284.

Zhao, L., Jin, J., Wang, S.-Y., and Ek, M.B. (2012). Integration of remote-sensing data with WRF to improve lake-effect precipitation simulations over the Great Lakes region. *Journal of Geophysical Research* **117**, D09102, doi: 10.1029/2011JD016979.

Acronyms

ALOS	Advanced Land Observing Satellite
AMSR-E	Advanced Microwave Scanning Radiometer–Earth Observing System
AMSU	Advanced Microwave Sounding Unit
ASAR	Advanced Synthetic Aperture Radar

ASTER	Advanced Spaceborne Thermal Emission and Reflection Radiometer
AVHRR	Advanced Very High Resolution Radiometer
CIS	Canadian Ice Service
CLIMo	Canadian Lake Ice Model
Envisat	Environmental Satellite
ERS-1/2	European Remote Sensing satellite-1/2
ETM+	Enhanced Thematic Mapper Plus
FLake	Freshwater Lake model
GBL	Great Bear Lake
GFO	Geosat Follow-On satellite
GLAWEX'97	Great LAkes Winter Experiment
GOES	Geostationary Operational Environmental Satellites
GSL	Great Slave Lake
HH	Co-polarization (horizontal send – horizontal receive)
HV	Cross-polarization (horizontal send – vertical receive)
IGOS	Integrated Global Observing Strategy
IMS	Interactive Multisensor Snow and Ice Mapping System
IRGS	Iterative Region Growing with Semantics algorithm
JAXA	Japan Aerospace eXploration Agency
JERS-1	Japanese Earth Resources Satellite 1
JPL	Jet Propulsion Laboratory
LST	Lake surface temperature
MAGIC	Map-Guided Ice Classification System software
MBE	Mean Bias Error
MERIS	MEdium Resolution Imaging Spectrometer
MetOp	Meteorological Operational satellite program
MODIS	Moderate Resolution Imaging Spectroradiometer
NARR	North American Regional Reanalysis
NASA	National Aeronautics and Space Administration
NIC	National Ice Service, U.S.
NOAA	National Oceanic and Atmospheric Administration
NWP	Numerical Weather Prediction
PALSAR	Phased-Array type L-band SAR
PRISM	Panchromatic Remote Sensing Instrument for Stereo Mapping
QuikSCAT	Quick Scatterometer
RADARSAT	Radar Satellite of the Canadian Space Agency
RCM	Regional Climate Model
RMSE	Root Mean Square Error
SAR	Synthetic Aperture Radar
SMMR	Scanning Multi-channel Microwave Radiometer
SPOT-5	Système Pour l'Observation de la Terre
SSM/I	Special Sensor Microwave/Imager
SWE	Snow Water Equivalent

TB	Brightness temperature
TM	Thematic Mapper
TOPEX	TOPography EXperiment
USAF	United States Air Force
VGT VEGETATION	Sensor on SPOT satellite
VV	Co-polarization (vertical send – vertical receive)

Websites cited

http://www.natice.noaa.gov/products/great_lakes.html
http://earthobservatory.nasa.gov/IOTD/view.php?id=81227
http://earthobservatory.nasa.gov/IOTD/view.php?id=81227